Organic Halides and Nanocone Plastic Structures Enhance the Energy Conversion Efficiency and Self-Cleaning Ability of Colloidal Quantum Dot Photovoltaic Devices

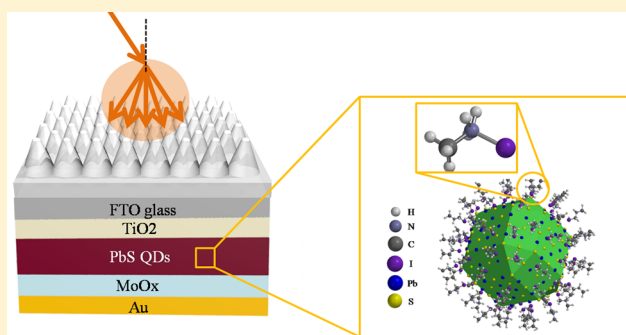Mohammad Mahdi Tavakoli,[†,‡] Abdolreza Simchi,*[,†,§] Rouhollah Tavakoli,[†] and Zhiyong Fan*[,‡]

[†]Department of Materials Science and Engineering, Sharif University of Technology, 14588 Tehran, Iran
[‡]Department of Electronic and Computer Engineering, Hong Kong University of Science and Technology, Clear Water Bay, Kowloon, Hong Kong
[§]Institute for Nanoscience and Nanotechnology, Sharif University of Technology, 14588 Tehran, Iran

S *Supporting Information*

ABSTRACT: This paper presents solid-state ligand exchange of spin-coated colloidal lead sulfide quantum dot (PbS QD) films by methylammonium iodide (MAI) and integration of them in depleted heterojunction solar (DHS) devices having an antireflecting (AR) nanocone plastic structure. Time-resolved photoluminescence measurements determine a shorter lifetime of the charge carries on a semiconductor (TiO_2) electron transfer layer for the MAI-passivated QD films as compared with those with long-chain aliphatic or short thiol ligands. Consequently, the DHS device yields improved power conversion efficiency (>125%) relative to oleic-acid-passivated PbS QD films. Using anodized aluminum oxide templates, an inverted nanocone polydimethylsiloxane structure was also prepared and utilized as an AR layer in the DHS device. The solar cells exhibit an energy conversion efficiency of 7.5% with enhanced water-repellant ability.

INTRODUCTION

Lead chalcogenide quantum dots (QDs) have attracted significant attention for optoelectronic devices such as lasers, light-emitting diodes (LEDs), and solar cells due to their low-cost fabrication process, band-gap tunability, and high carrier mobility.[1−3] In these nanocrystals, the confinement of carriers coupled to the QD lattice results in an excess energy that enlarges the band gap and discretizes the density of states compared with the bulk material. This causes a larger overlap of wave functions for electron and hole, resulting in a higher absorption coefficient.[4−6] Moreover, in several QD systems with lead chalcogenides, carrier multiplication (CM) or multiple exciton generation (MEG) as well as hot carrier phenomena have been observed.[7,8] These objects could allow breaking the Shockley−Queisser (SQ) limit in a solar cell device.[9] Despite these great advantages, QDs have a large surface area with a high density of trap states originating from their surface dangling bonds,[10,11] which increases the possibility of charge recombination and reduces the optoelectronic device performance.[12] To overcome this shortcoming, several strategies such as surface passivation by organic ligands,[13−16] atomic passivation by halides,[17] incorporation of graphene,[18−20] and doping with low electron affinity metals[21,22] have been examined. Therefore, layer-by-layer chemical processing of PbS colloidal quantum dot (CQD) films to exchange long aliphatic

ligands by short organic molecules, such as mercaptopropionic acid (MPA),[23−25] have become a gold standard procedure to fabricate high-performance CQD solar cells.[26−29] In fact, the carriers transport inside the CQD film crucially depends on the distance between QDs, which is corresponded to the length of organic ligands as well as the presence of the midgap trap states, combined with disorders and imperfect surfaces.[30,31] In recent years, the power conversion efficiency (PCE) of PbS CQD devices has surged dramatically to >11% through surface modifications of QDs as well as band-gap engineering of the QD films.[32] However, the current performance of these devices is well below the SQ efficiency limit,[33] which encourages further investigation. The lower PCE of the devices is also attributed to the near- and mid-infrared absorption capacity of the QD film.[34] Therefore, new strategies have to be taken into account to increase the light absorption efficiency of the CQD film with a controlled thickness with regard to the recombination of charge carriers. On the contrary, in a solar farm, the surface of solar panels is always contaminated by accumulated dust and impurities, which reduces the device performance. Therefore, water-repellant and self-cleaning

 9757
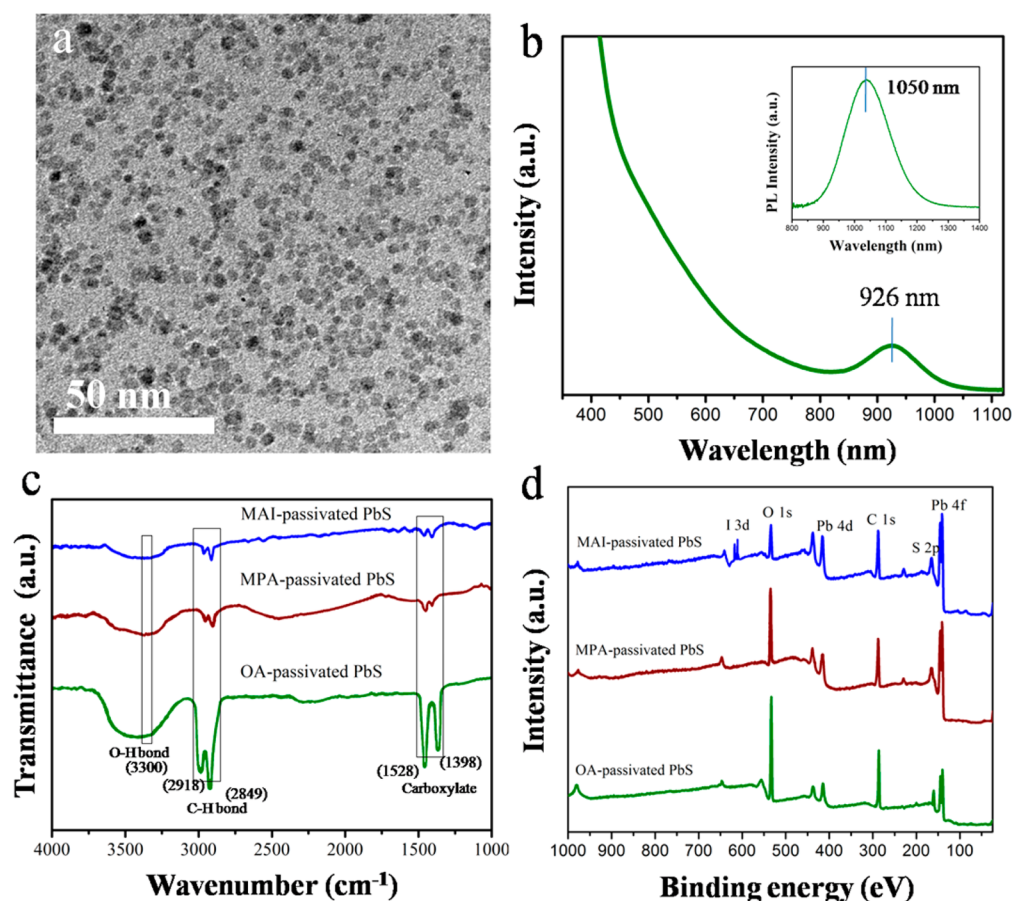
Figure 1. Characterization of OA-passivated PbS QDs prepared by the hot injection method and the quantum-dot films fabricated through a layer-by-layer spin coating procedure. (a) TEM image of OA-passivated PbS QDs shows that uniform QDs with an average diameter of 3 nm and narrow size distribution (±1.5 nm) are synthesized. (b) Absorption and emission peaks (inset) of OA-passivated PbS QDs determine that QDs are light-active in the near- and mid-infrared regions. (c) FTIR and (d) XPS spectra of PbS QDs before and after ligand exchange reveal successful replacement of OA with MPA and MAI through the layer-by-layer ligand processing.

ability of the solar panels are very important to carry away dust by water droplets upon rainfall.

Herein we employ a chemical ligand based on organic halides to passivate the surface dangling bonds and trap states of PbS QDs using solid-state ligand exchange method. Methylammonium iodide (MAI), which is frequently used for the synthesis of perovskite materials,[35,36] can replace long aliphatic ligand (oleic acid) in the QD films by a facile solid-state chemical processing. Recently, MAI passivation of PbS CQDs has been reported. For instance, Lan et al.[3] synthesized stable MAI-PbS CQDs in a solution phase and deposited them by spin coating to study the quality of the films; Balazs et al.[13] studied the effect of different ligands (including MAI) on the quality of PbS films prepared by combined blade coating and dip coating. In the present work, we used a layer-by-layer spin-coating technique to replace long-chain aliphatic ligands by MAI through the solid-state ligand-exchange procedure. It is shown that MAI-passivated PbS QD films have a lower recombination and charge-transfer resistance compared with the passivated dots by MPA and OA, yielding a higher PCE. Furthermore, the light absorption efficiency in the PbS QD films is enhanced through a 3D plastic nanostructure fabricated in nanocone shape on an anodized aluminum oxide (AAO) thin film. This nanostructure is attached to the fluorine-doped tin oxide (FTO) glass to provide antireflection (AR) and self-cleaning properties. Ultraviolet−visible spectrometry and measurement of the

external quantum efficiency (EQE) indicate that light management by the plastic nanostructure improves the light absorption in the infrared range. Combined passivation of the PbS QDs by MAI and enhanced light absorption increases PCE to 7.5%, which is ~21% higher than MPA-passivated PbS CQD solar cells.

■ RESULTS AND DISCUSSION

To fabricate CQD devices, OA-passivated QDs were synthesized by the hot injection method, as described in the Experimental Section. The QDs were then deposited on TiO₂-coated FTO glasses through a layer-by-layer spin-coating process to prepare thin films of ~300 nm thickness. A solid-state ligand exchange approach was employed to replace long OA chains with shorter ligands of MPA and MAI. The characteristics of the prepared QDs and films are shown in Figure 1. TEM study determined that the QDs had an average diameter of ~3 nm with a narrow size distribution (Figure 1a and Figure S1a). At high magnifications, crystalline particles with an interplanar spacing of 0.295 nm were observed (see Figure S1b). This is the distance between two (200) planes of the cubic lead sulfide structure.[3] Further evaluation by X-ray diffraction (XRD) analysis and energy-dispersive X-ray spectrometry (EDS) supported the formation of crystalline PbS particles (see Figure S2a,b, respectively). The UV−vis spectrum of the QDs (Figure 1b) shows a well-defined

9758
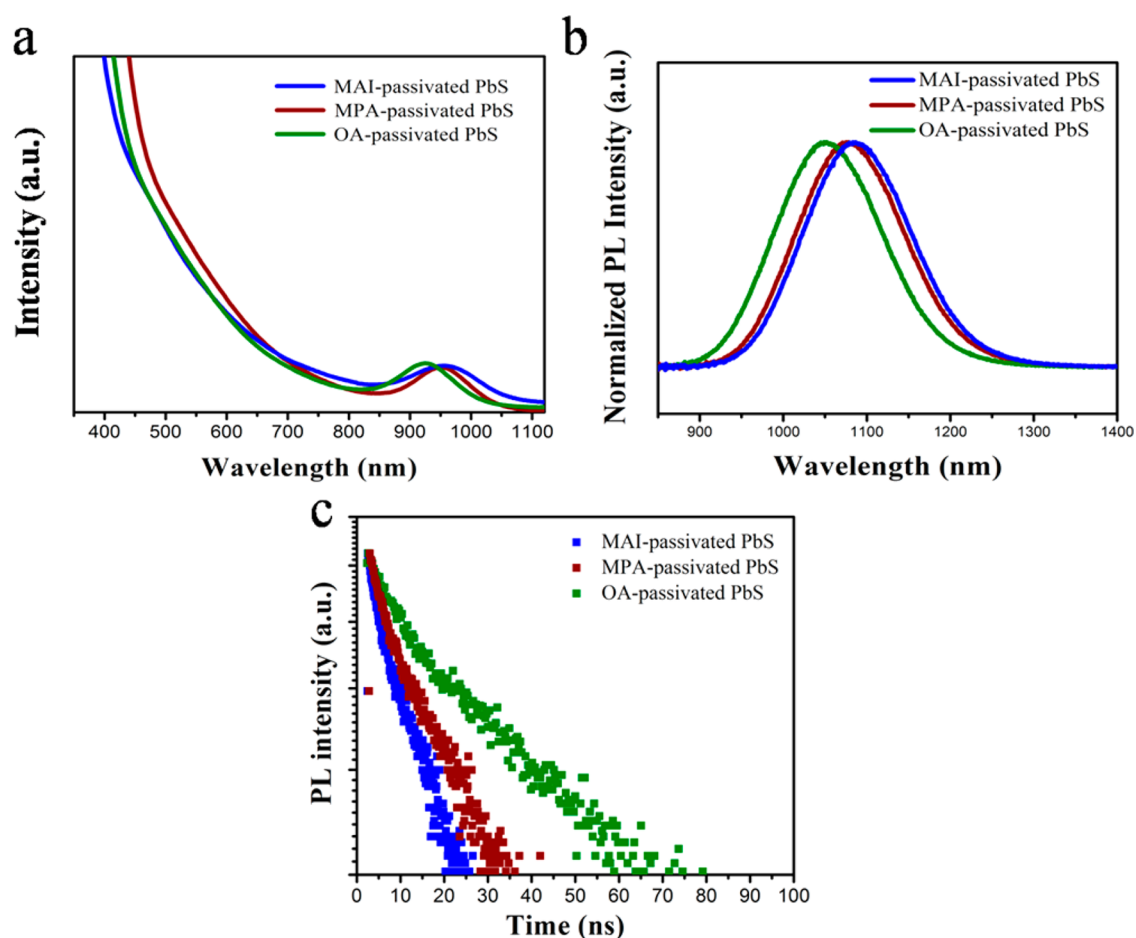
Figure 2. (a) Absorption and (b) steady-state PL emission (excited at 405 nm) of quantum-dot films deposited on TiO$_2$ ETL indicate a red shift in the spectra. (c) TRPL spectra of quantum dot films on TiO$_2$-coated FTO glass before and after the ligand exchange.

excitonic peak at 926 nm with a photoluminescence (PL) emission peak of 1050 nm (see the inset). The absorption peak position determines an optical band gap of 1.34 eV based on the Moreels equation.[37] On the contrary, the strong emission peak reveals efficient passivation of the dangling bonds with OA ligands,[27] as revealed in their Fourier transform infrared (FTIR) spectrum (Figure 1c).

Herein, the peaks at around 1398 and 1528 cm^{-1} correspond to the carboxylate group, and two others near 2849 and 2918 cm^{-1} are ascribed to the CH$_2$ bonds.[38,39] After the ligand passivation with MPA and MAI, the peak intensity of the carboxylate and CH$_2$ groups of PbS QDs is decreased drastically, which indicates the removal of the OA molecules from the surfaces. As reported in the literature, MPA molecule itself has a peak at 2557 cm^{-1} that is ascribed to the oscillation mode of thiol (−SH) group.[21,31] This peak is not appeared in the IR spectrum of MPA-passivated PbS QDs, indicating the reaction of thiol group with the surface of PbS QDs. Additionally, the vibration peaks located at 3300 cm^{-1} (for hydroxyl (−OH) group) in the MPA passivated PbS QDs show the existence of MPA and OA on the surface of PbS QDs.[31] However, the intensity of this peak is reduced after passivation of PbS QDs with MAI molecules. In fact, the MAI sample only shows carboxylate and C−H bonds with very low intensity, revealing the high degree of ligand exchanging. This finding is further confirmed by X-ray photoelectron spectroscopy (XPS), as shown in Figure 1d. The presence of iodide peak at 619.4 eV

indicates bonding of iodide to the surface of QDs. In addition, the presence of oxygen on the surface of PbS QDs is evidence, showing the passivation of dots with OA and MPA, as reported in our previous works.[19,20] To further study the ligand exchange process, atomic ratios from XPS spectra were calculated by integrating the area under each peak and atomic sensitivity factors, followed by normalization of these numbers using OA-passivated PbS QDs sample. The results show that 59 and 71% of initial oleic acid ligands are replaced by MPA and MAI molecules, respectively, suggesting the highest incorporation of MAI molecules on the surface of QDs.

To study the optical properties of the QD films, their absorption and emission in a wide range of the spectrum were measured by UV−vis near-infrared, steady-state PL, and time-resolved photoluminescence (TRPL) spectroscopies, as shown in Figure 2. The effect of ligand passivation on the optical properties of the films (300 nm thickness) is shown in Figure 2a,b. It is observed that the ligand passivation with the smaller organic molecules causes a red shift in the absorption peak, revealing more compactness of QDs in the film, that is, shorter interparticle spacing.[20] The MAI treatment induces more red shift in the absorption spectrum as compared with MPA, which may be ascribed to shorter particle distances. The steady-state PL spectra of the QD films are consistent with the results of UV−visible spectrometry.

To further elucidate the effect of MAI ligand on the optical properties of PbS CQDs, the ligand-exchange process was
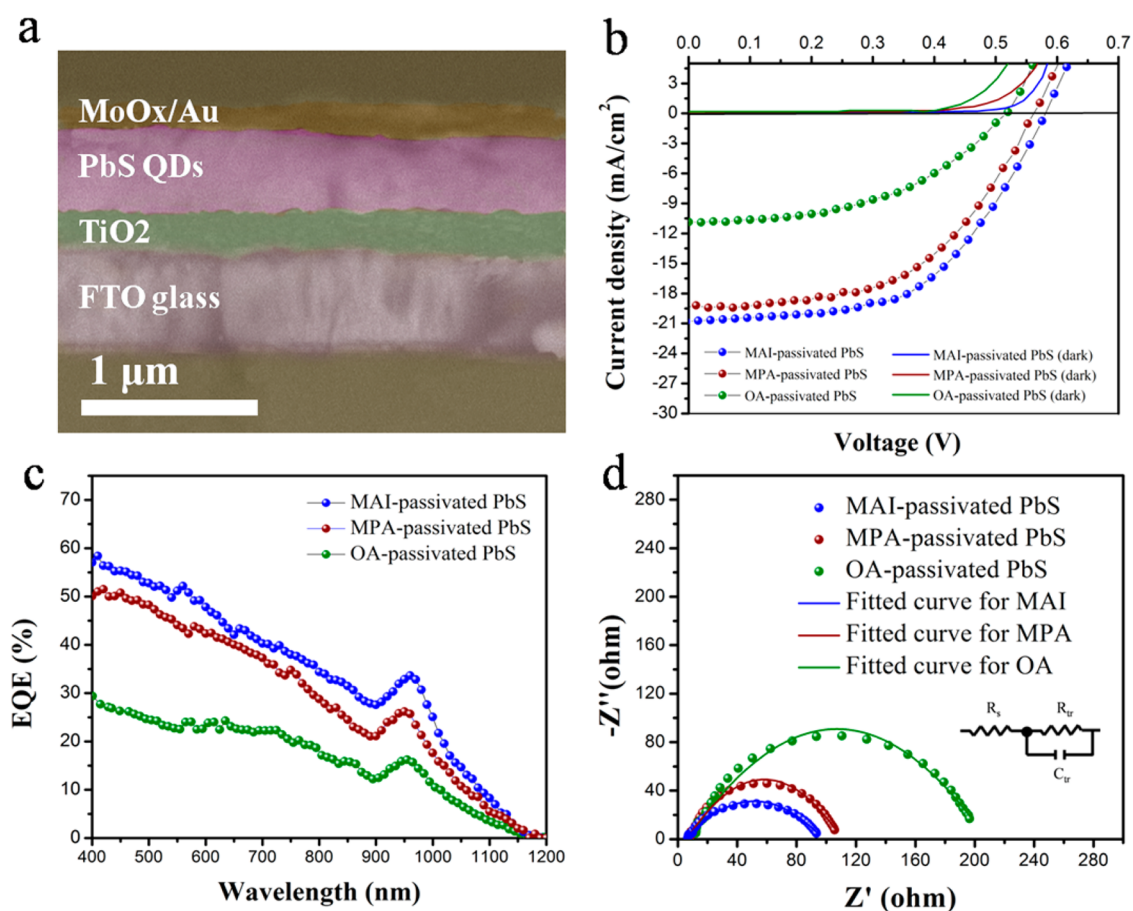
Figure 3. (a) Cross-sectional SEM image show the architecture of PbS CQD solar cell device. (b) $J-V$ curves under 1.5 AMG and dark current indicate the photovoltaic performance of the heterojunction devices. (c) EQE spectra determine the effect of organic molecules on the quantum efficiency of the devices. (d) EIS spectra of the photovoltaic devices after fitting determine the charge transfer and carrier collection resistance of the films.

Table 1. Figure of Merits for the Prepared Photovoltaic Devices Showing the Effect of Surface Passivation, the Type of Ligands, and AR Film on the Performance of PbS CQDs (Number of Devices = 10)

passivated by	V_{oc} (V)	J_{sc} (mA/cm^2)	FF (%)	PCE (%)	R_s (Ω)	R_{ct} (Ω)
oleic acid (OA)	0.52 ± 0.03	10.9 ± 1.8	54 ± 4	3.1 ± 0.5	10.5	192
mercaptopropionic acid (MPA)	0.56 ± 0.02	19.2 ± 1.4	58 ± 2	6.2 ± 0.3	8.7	98
methylammonium iodide (MAI)	0.58 ± 0.03	20.7 ± 1.3	59 ± 3	7.0 ± 0.2	7.8	86
methylammonium iodide (MAI) + AR film	0.58 ± 0.07	21.9 ± 1.1	59 ± 3	7.5 ± 0.2		

performed in solution, as reported in the literature.[3] Measurements of the photoluminescence quantum efficiency (PLQE) determine that PbS CQDs passivated by OA, MPA, and MAI have PLQE of 25, 30, and 32%, respectively. Therefore, the isolated MAI-passivated PbS QDs have a higher radiative PL in the colloidal form. This suggests that MAI molecules passivate surface trap states and recombination sites of the dots efficiently, making it a good candidate for the fabrication of solar cell devices.

To investigate the usability of the MAI-passivated PbS QDs for solar cell devices, the quenching effect of QD films on an ETL layer was studied. The QD films having different ligands were prepared by the layer-by-layer spin-coating method. Figure 2c shows the results of TRPL measurement. The fitting parameters of the TRPL results are shown in Table S1. Note that a lower lifetime determines a high rate of electron transfer between the absorber layer and ETL.[23−25] It is seen that the MAI-passivated QD film deposited on TiO$_2$ ETL has the shortest carrier lifetime, indicating faster carrier extraction with lower recombination rate in the QD film. The MPA-treated film exhibits longer carrier lifetime than MAI but shorter than OA, indicating that OA-treated film has the slowest carriers extraction. This finding is consistent with the length of the organic molecules, $l_{MAI} < l_{MPA} < l_{OA}$, which affects the compactness of the films as well as their passivation ability of the surface dangling bonds.[28] Different studies[3,17,27] have shown that amine groups and halides effectively passivate the deep midgap trap states of PbS QDs, thereby reducing the recombination rate of charge carries with enhanced transportation rate. The presented results so far determine that the surface dangling bonds are passivated more effectively by MAI as compared with MPA and OA ligands.

To further study the effect of MAI treatment on the photovoltaic performance, DHS PbS CQD solar cells were fabricated. As shown in Figure 3a, the device architecture consisted of the FTO glass covered with a thin film of TiO$_2$ a
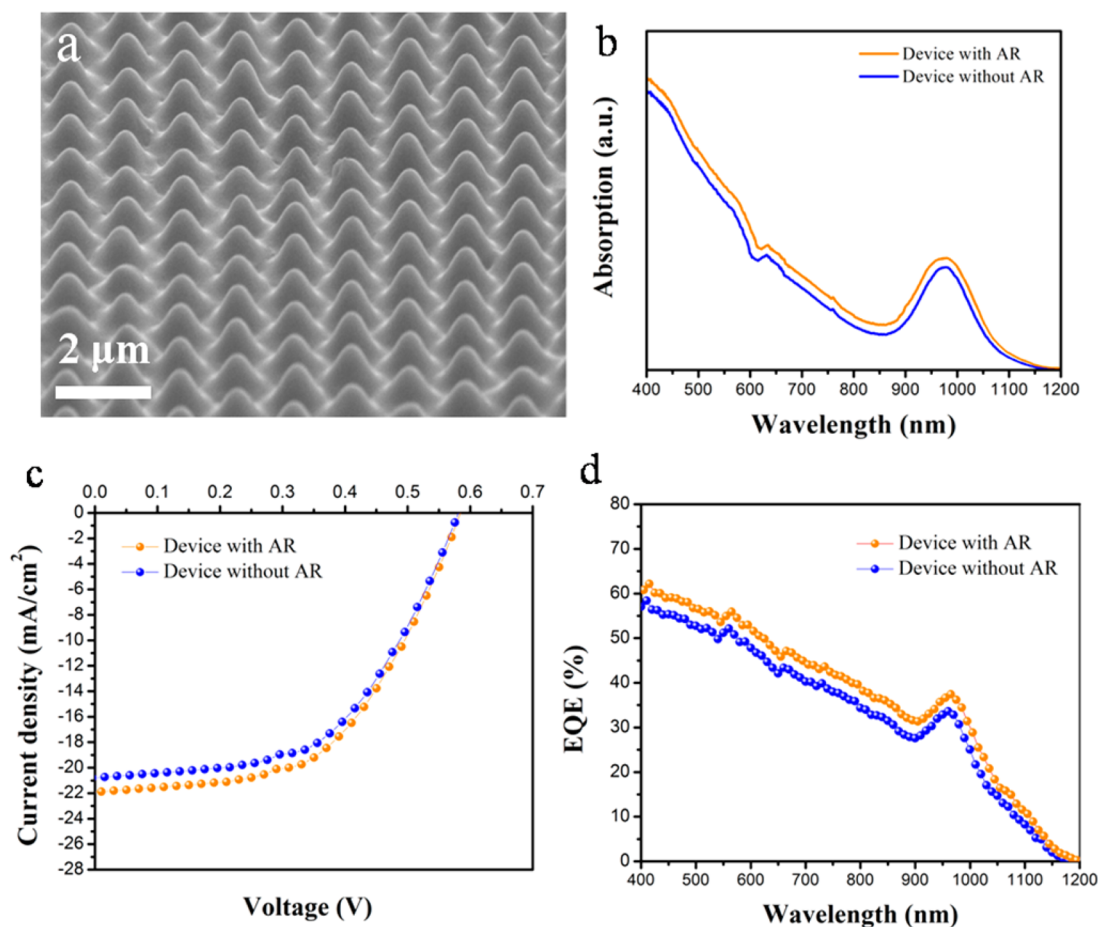
Figure 4. (a) Angular-view SEM image of the PDMS nanocone array with an aspect ratio of 1.0. (b) Effect of nanocone array on the absorption spectrum of PbS CQD film. (c) $J-V$ curves of MAI-passivated quantum dot films with and without the plastic nanostructure. (d) EQE spectra of the device show the effect of nanocone array on the current density of the solar cells in the entire wavelength.

blocking layer (~200 nm), PbS CQD film (~300 nm), hole-transfer layer (15 nm, MoO_x), and gold contact (100 nm). The current density–voltage ($J-V$) curves of the devices under simulated (AM1.5G) solar irradiation and for dark current are shown in Figure 3b. Table 1 presents the figures of merit for the prepared cells. The better energy conversion performance of the MAI-treated film is notable. Both open-circuit voltage (V_{oc}) and short-circuit current (J_{sc}) are increased when the long OA ligand is replaced by the smaller organic molecules. This is basically because of shorter interparticle spacing, which boosts the carrier transportation, while the higher V_{oc} demonstrates better passivation of midgap trap states.[28] MAI treatment particularly affects the transport of charge carriers as compared with MPA without a major influence on V_{oc}. To have a better understanding of the role of ligands on V_{oc}, the dark current of devices versus applied voltage is plotted on a logarithmic scale in Figure S3. As seen, MAI-passivated PbS QDs show the highest V_{oc} compared with its counterparts. As reported in the literature,[3,27] iodide is highly appropriate for the surface passivation of PbS QDs, and the MAI treatment incorporates the highest amount of iodide in the QD film. As compared with MPA, recombination sites in PbS QDs are well-passivated by iodide, so that improved photovoltaic properties are attained. Moreover, MAI molecules are shorter than MPA, which would result in a film with more compactness (as evidenced by the red shift in absorption spectrum). In order to support this finding, EQE of the cells was recorded (Figure 3c). The higher EQE of

the MAI-treated device determines that the utilized organic halide molecule more effectively passivated the deep midgap trap states, which directly affects the quantum efficiency and transport properties. The results of electrochemical impedance spectroscopy (EIS) are shown in Figure 3d. The Nyquist curves present Z' versus $-Z''$, which are the real and imaginary parts of the cell impedance, respectively. Using the curve fitting method, the series (R_S) and shunt (R_{ct}) resistances were determined (Table 1). The results determine the effect of ligand passivation on the charge collection via reducing the charge-transfer resistance. Notably, the MAI-passivated PbS CQD device has the smallest semicircle radius with lower R_s (7.8 Ω) and R_{ct} (86 Ω). Therefore, the MAI treatment not only affects the optical properties of the quantum films but also influences the carrier collection. We have found that MAI treatment boosts PCE of the photovoltaic device from 3.1% (for OA-passivated PbS) to 7.0%, which is 13% higher than MPA treatment.

Recent studies[35,37] have shown that 3D electrodes as well as AR nanostructures have a promising potential in improving the light-harvesting capability and thus the performance of solar cell devices. In the present work, for the first time, we have employed a regular nanocone array on the front bottom side of the FTO glass for light management throughout PbS QD films. This nanostructure also provides water-repellent and self-cleaning functions to the device. As aforementioned, these features are very important for practical applications of the
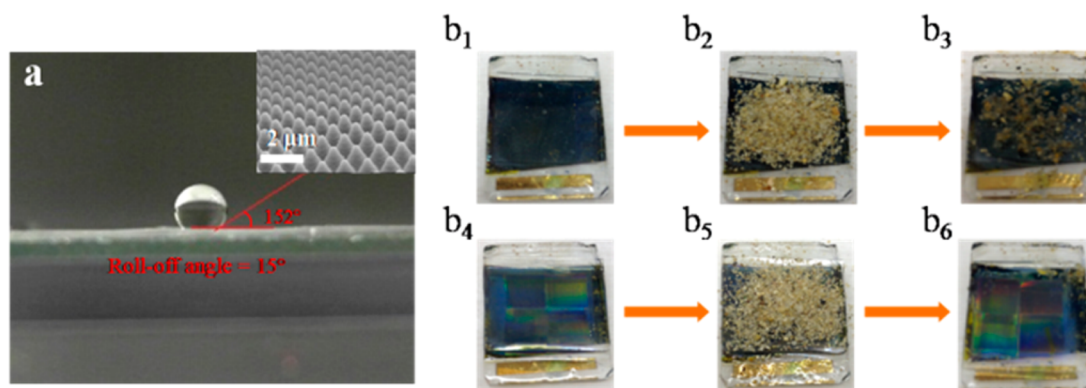
Figure 5. (a) Photograph shows a drop of water on the surface of the nanocone PDMS array with static contact angles of 152° and roll-off angle of 15°. The inset is a cross-sectional SEM image of the nanocone array. (b) Self-cleaning experiment on the PbS CQD devices without (b_1, b_2, b_3) and with (b_4, b_5, b_6) the plastic nanostructure.

photovoltaic devices in solar farms. An SEM image of the utilized AAO mold is shown in Figure S4. The inverted nanocone structure of the PDMS antireflection film is shown in Figure 4a. The cones have a depth and opening width of 1 μm (aspect ratio of 1), which effectively influence the light-harvesting capacity of solar cell devices, as shown elsewhere.[40−45] The effect of the nanocone array on the light absorption capacity of the photovoltaic devices is shown in Figure 4b, as an example for the MAI-passivated PbS QDs. The absorption spectrum is upshifted through the entire spectrum of light from 400 to 1200 nm. Figure 4c shows the effect of nanocone array on the J−V curves of the representative device under 1 sun simulated illumination. Table 1 presents the average characteristics for $n = 10$ photovoltaic devices. As seen in Figure 4d, the nanocone array slightly increases EQE in the entire wavelength due to the enhanced light absorption in the QD film. As a result, PCE of the solar device is enhanced to 7.5%, which is ~21% higher than the MPA-passivated cell without employing the plastic nanostructure. To show the self-cleaning capacity of the nanocone array, a drop of water was placed on the surface and the contact angle was measured (Figure 5a). The contact angle and roll-off angle are 152 and 15°, respectively. This observation determines that the nanocone film is superhydrophobic, which enables us to provide self-cleaning capacity to the photovoltaic device.[36] Figure 5b presents a self-cleaning experiment by spreading sand particles on the top surface of the cells covered with the nanocone plastic structure. This experiment shows that the sand particles can easily be removed by rolling a water droplet across the surface, unlike the device without the plastic nanostructure. Such self-cleaning property is highly desirable to improve the long-term stability of QD solar devices because any impurity such as dust can stick to the device in the ambient air and block the sun light, which decreases the device performance.[36]

CONCLUSIONS

In summary, we employ MAI as a chemical ligand for the surface passivation of PbS QDs using solid-state ligand-exchange method through a layer-by layer spin coating process. Compared with MPA, MAI molecules more effectively passivate the deep trap-states and provide better charge-carrier transportation. The steady-state and transient PL measurements on the MAI-passivated PbS CQD film also indicate higher red shift in the emission peak with better quenching

effect on ETL. Consequently, analysis of the J−V plots and EQE spectra demonstrates that the device based on MAI has a higher short-current density with better photovoltaic performance (13% improvement). To further improve PCE, an inverted nanocone array of PDMS fabricated by AAO template was prepared and stacked to the FTO glass for more efficient light management. The plastic nanostructure has a contact angle and roll-off angle of 152 and 15°, respectively. This superhydrophobicity adds self-cleaning ability to the photovoltaic devices along with enhanced PCE by 21% relative to MPA-passivated cells.

EXPERIMENTAL SECTION

Materials. Lead(II) oxide powder (PbO, 99%), oleic acid (OA, technical grade 90%), anhydrous toluene, octane, methanol, isopropyl alcohol, and Triton X-100 were purchased from Merck, Germany. Bis(trimethylsilyl) sulfide (TMS, Strem, 97% purity), 1-octadecene (ODE, Sigma-Aldrich, technical grade 90%), MPA (Sigma-Aldrich), MAI (Dyesol), TiO$_2$ paste (Dyesol 18NRT, Dyesol), and titanium tetrachloride (Sigma-Aldrich) were used as received without further purification.

Synthesis of Lead Sulfide Quantum Dots. PbS CQDs was synthesized via the hot injection method.[37,38] First, 210 μL of TMS was dissolved in 10 mL of ODE. Then, this solution was quickly injected into a three-necked flask containing 0.45 g of PbO and 18 mL of ODE after mixing at 110 °C for 16 h. The reaction was completed after 10 min at 120 °C. The reaction product was washed several times by centrifugation (4000 rpm), using methanol and acetone, and finally redispersed in octane (80 mg/mL).

Device Fabrication. The solar cell device was fabricated on FTO glasses with ohmic sheet resistance of 8 Ω (Hartford Glass, USA). First, the substrates were cleaned by deionized (DI) water (Milipore, 18 MΩ-cm) containing 3 vol % Triton X-100, isopropanol, and acetone through sonication for 30 min, followed by drying by a nitrogen flow. Then, a solution of TiO$_2$ nanoparticles (30 nm, 18NRT, Dyesol) was spin-coated on the FTO glass at 4000 rpm for 40 s to obtain 200 nm thick mesoporous layer. Afterward, the layer was dried at 125 °C for 10 min, followed by annealing at 500 °C for 30 min. The TiO$_2$ layer was then treated by immersing the substrates into an aqueous solution of 50 mM TiCl$_4$ for 30 min at 75 °C. Finally, the substrates were washed and annealed at 550 °C for 30 min in air. A layer-by-layer deposition technique combined with a solid-state ligand exchange method was utilized to deposit PbS

QDs on the FTO/TiO_2 substrate and replace the long OA ligands with short molecules of MPA and MAI. Herein the PbS CQDs were spin-coated at 2500 rpm for 30 s and washed with an MPA solution (1 vol % in anhydrous methanol) or an MAI solution (10 mM in IPA/chloroform (2:1 vol %)), spin-coated once more at 2500 rpm for 10 s, and finally washed with anhydrous methanol. The process was repeated 10 times to obtain a uniform layer of PbS QDs with ~300 nm thickness. After drying, the top contact consisting of MoO_3/Au layers (15 nm/100 nm) was thermally evaporated at a rate of 0.8 Å s^{-1} to complete the device fabrication.

Fabrication of Nanocone Plastic Nanostructure. To fabricate AR film, AAO template was employed. First, an aluminum foil (0.25 mm thick, 99.99% purity, Alfa Aesar) was electro-polished and then imprinted using a hexagonally ordered nanopillars silicon stamp with a height of 200 nm and a pitch of 1 μm. Afterward, the patterned foil was anodized in a solution containing 230 mL 1:1, 4 wt % citric acid/ethylene glycol (EG) + 15 mL 0.1% H_3PO_4 under 400 V DC and finally etched in a mixture of phosphoric acid (6 wt %) and chromic acid (1.8 wt %).[36] This process repeated several times to obtain an inverted nanocone (i-cone) array (see Figure S4). This pattern was then covered by a 30 nm thick gold as an antisticking layer using the thermal evaporation process. Finally, a PDMS solution (Sylgard 184, Dow Corning 10:1 ratio with the curing agent) was drop-casted on the Au-coated i-cone template, followed by degassing. After curing the sample at 80 °C for 2 h, the PDMS nanocone pattern with a thickness of 0.2 mm was peeled off from the i-cone mold.

Materials Characterizations. The prepared dots were analyzed by high-resolution transmission electron microscopy (HRTEM, JOL, JEM-2100, Japan) equipped with an EDS as well as the XRD method (Stone Sandi P, USA) utilizing a Cu Kα radiation. A PerkinElmer Fourier transform infrared spectrometer (FTIR, Spectrum RX, USA) was utilized to measure infrared spectra. XPS were recorded by a hemispherical analyzer with an Al Kα X-ray source (1486.6 eV) operated at 10^{-7} Pa. The light absorption and PL spectra were measured by using a Varian Carry 500 spectrometer (Varian, USA) and an FLS920P fluorescence spectrometer (Edinburgh Instruments), respectively. The PL setup was equipped with a cryogenically cooled photomultiplier (R5509-43, Hamamatsu) with a 450 W continuous xenon arc lamp as the excitation source (excitation wavelength was 670 nm) for steady-state spectra and a picosecond pulsed diode laser (EPL-405, excitation wavelength 405 nm, pulse width: 49 ps) for lifetime measurements. The following exponential function $I(t) = B_1 e^{-t/\tau_1} + B_2 e^{-t/\tau_2} + B_3 e^{-t/\tau_3}$ was employed for curve fitting of PL decay curves, where τ_i and B_i are $1/e$ lifetime constant and the amplitude of exponential terms, respectively. The average lifetimes were estimated by the formula $\tau_{avg} = \frac{B_1 \tau_1^2 + B_2 \tau_2^2 + B_3 \tau_3^2}{B_1 \tau_1 + B_2 \tau_2 + B_3 \tau_3}$.

The PLQE was measured using the fluorescence spectrometer equipped with an integrating sphere with BENFLECR-coated inner face (Edinburgh Instruments). To study the thickness, morphology, and roughness of the films, field-emission scanning electron microscopy (FESEM, Hitachi S4160, Japan) was utilized. For EIS, an Autolab PGSTAT30 instrument (EcoChemie, Utrecht, Netherlands) with a frequency range from 1 MHz down to 0.1 Hz at bias potentials of 0.6 V (with a 10 mV sinusoidal AC perturbation) was utilized. All measurements were done at room temperature.

Photovoltaic Performance. To record current density–voltage ($J–V$) data at AM1.5G, a solar simulator with a Xe lamp, filters (with an intensity of 100 mW cm^{-2}) and a Keithley 2400 (USA) instrument were employed. The range of voltage was between −1 and +1 V. The step size and delay time were 0.02 V and 150 ms at each point, respectively. The power measurement accuracy was expected to be ±5%. To calculate EQE versus wavelength, an array of white LEDs with a constant white-light bias of ~5 mW cm^{-2} was used. A 300 W xenon lamp (ILC Technology) was focused through a Gemini-180 double monochromator (Jobin Yvon) to provide the excitation beam and then chopped at ~2 Hz. A Model SR830 DSP lock-in amplifier was used to record the signal.

■ ASSOCIATED CONTENT

Ⓢ Supporting Information

The Supporting Information is available free of charge on the ACS Publications website at DOI: 10.1021/acs.jpcc.7b02394.

XRD pattern, TEM image and analysis of PbS QDs, TRPL fitting parameters, and SEM image of the mold for fabrication of antireflection. (PDF)

■ AUTHOR INFORMATION

Corresponding Authors
*A.S.: E-mail: simchi@sharif.edu. Tel: +98 (21) 6616 5261. Fax: +98 (21) 6600 5717.
*Z.F.: E-mail: eezfan@ust.hk.

ORCID ⃝
Mohammad Mahdi Tavakoli: 0000-0002-8393-6028
Zhiyong Fan: 0000-0002-5397-0129

Notes
The authors declare no competing financial interest.

■ REFERENCES

(1) Shirasaki, Y.; Supran, G. J.; Bawendi, M. G.; Bulović, V. Emergence of colloidal quantum-dot light-emitting technologies. *Nat. Photonics* **2012**, *7*, 13−23.

(2) Hines, M. A.; Scholes, G. D. Colloidal PbS nanocrystals with size-tunable near-infrared emission: observation of post-synthesis self-narrowing of the particle size distribution. *Adv. Mater.* **2003**, *15*, 1844−1849.

(3) Lan, X.; Voznyy, O.; García de Arquer, F. P.; Liu, M.; Xu, J.; Proppe, A. H.; Walters, G.; Fan, F.; Tan, H.; Liu, M.; et al. 10.6% certified colloidal quantum dot solar cells via solvent-polarity-engineered halide passivation. *Nano Lett.* **2016**, *16*, 4630−4634.

(4) Debellis, D.; Gigli, G.; Ten Brinck, S.; Infante, I.; Giansante, C. Quantum-confined and enhanced optical absorption of colloidal PbS quantum dots at wavelengths with expected bulk behavior. *Nano Lett.* **2017**, *17*, 1248.

(5) Fu, X.; Pan, Y.; Wang, X.; Lombardi, J. R. Quantum confinement effects on charge-transfer between PbS quantum dots and 4-mercaptopyridine. *J. Chem. Phys.* **2011**, *134*, 024707.

(6) Rossetti, R.; Nakahara, S.; Brus, L. E. Quantum size effects in the redox potentials, resonance Raman spectra, and electronic spectra of CdS crystallites in aqueous solution. *J. Chem. Phys.* **1983**, *79*, 1086–1088.

(7) Gesuele, F.; Sfeir, M. Y.; Koh, W. K.; Murray, C. B.; Heinz, T. F.; Wong, C. W. Ultrafast super continuum spectroscopy of carrier multiplication and biexcitonic effects in excited states of PbS quantum dots. *Nano Lett.* **2012**, *12*, 2658–2664.

(8) El-Ballouli, A. A. O.; Alarousu, E.; Usman, A.; Pan, J.; Bakr, O. M.; Mohammed, O. F. Real-time observation of ultrafast intraband relaxation and exciton multiplication in PbS quantum dots. *ACS Photonics* **2014**, *1*, 285–292.

(9) Midgett, A. G.; Luther, J. M.; Stewart, J. T.; Smith, D. K.; Padilha, L. A.; Klimov, V. I.; Nozik, A. J.; Beard, M. C. Size and composition dependent multiple exciton generation efficiency in PbS, PbSe, and PbS$_x$Se$_{1-x}$ alloyed quantum dots. *Nano Lett.* **2013**, *13*, 3078–3085.

(10) Gao, J.; Johnson, J. C. Charge trapping in bright and dark states of coupled PbS quantum dot films. *ACS Nano* **2012**, *6*, 3292–3303.

(11) McDonald, S. A.; Konstantatos, G.; Zhang, S.; Cyr, P. W.; Klem, E. J.; Levina, L.; Sargent, E. H. Solution-processed PbS quantum dot infrared photodetectors and photovoltaics. *Nat. Mater.* **2005**, *4*, 138–142.

(12) Graetzel, M.; Janssen, R. A.; Mitzi, D. B.; Sargent, E. H. Materials interface engineering for solution-processed photovoltaics. *Nature* **2012**, *488*, 304–312.

(13) Balazs, D. M.; Dirin, D. N.; Fang, H. H.; Protesescu, L.; ten Brink, G. H.; Kooi, B. J.; Kovalenko, M. V.; Loi, M. A. Counterion-mediated ligand exchange for PbS colloidal quantum dot superlattices. *ACS Nano* **2015**, *9*, 11951–11959.

(14) Ip, A. H.; Thon, S. M.; Hoogland, S.; Voznyy, O.; Zhitomirsky, D.; Debnath, R.; Levina, L.; Rollny, L. R.; Carey, G. H.; Fischer, A.; et al. Hybrid passivated colloidal quantum dot solids. *Nat. Nanotechnol.* **2012**, *7*, 577–582.

(15) Talapin, D. V.; Lee, J. S.; Kovalenko, M. V.; Shevchenko, E. V. Prospects of colloidal nanocrystals for electronic and optoelectronic applications. *Chem. Rev.* **2010**, *110*, 389–458.

(16) Wang, X.; Koleilat, G. I.; Fischer, A.; Tang, J.; Debnath, R.; Levina, L.; Sargent, E. H. Enhanced open-circuit voltage in visible quantum dot photovoltaics by engineering of carrier-collecting electrodes. *ACS Appl. Mater. Interfaces* **2011**, *3*, 3792–3795.

(17) Ning, Z.; Ren, Y.; Hoogland, S.; Voznyy, O.; Levina, L.; Stadler, P.; Lan, X.; Zhitomirsky, D.; Sargent, E. H. All-inorganic colloidal quantum dot photovoltaics employing solution-phase halide passivation. *Adv. Mater.* **2012**, *24*, 6295–6299.

(18) Tayyebi, A.; Tavakoli, M. M.; Outokesh, M.; Shafiekhani, A.; Simchi, A. Supercritical synthesis and characterization of graphene–PbS quantum dots composite with enhanced photovoltaic properties. *Ind. Eng. Chem. Res.* **2015**, *54*, 7382–7392.

(19) Tavakoli, M. M.; Tayyebi, A.; Simchi, A.; Aashuri, H.; Outokesh, M.; Fan, Z. Physicochemical properties of hybrid graphene–lead sulfide quantum dots prepared by supercritical ethanol. *J. Nanopart. Res.* **2015**, *17*, 1–13.

(20) Tavakoli, M. M.; Aashuri, H.; Simchi, A.; Kalytchuk, S.; Fan, Z. Quasi core/shell lead sulfide/graphene quantum dots for bulk heterojunction solar cells. *J. Phys. Chem. C* **2015**, *119*, 18886–18895.

(21) Thon, S. M.; Ip, A. H.; Voznyy, O.; Levina, L.; Kemp, K. W.; Carey, G. H.; Masala, S.; Sargent, E. H. Role of bond adaptability in the passivation of colloidal quantum dot solids. *ACS Nano* **2013**, *7*, 7680–7688.

(22) Tavakoli, M. M.; Aashuri, H.; Simchi, A.; Fan, Z. Hybrid zinc oxide/graphene electrodes for depleted heterojunction colloidal quantum-dot solar cells. *Phys. Chem. Chem. Phys.* **2015**, *17*, 24412–24419.

(23) Peng, Z.; Liu, Y.; Wu, L.; Zhao, Y.; Chen, K.; Chen, W. Influence of surface states of CuInS$_2$ quantum dots in quantum dots sensitized photo-electrodes. *Appl. Surf. Sci.* **2016**, *388*, 437–443.

(24) Xu, F.; Gerlein, L. F.; Ma, X.; Haughn, C. R.; Doty, M. F.; Cloutier, S. G. Impact of different surface ligands on the optical properties of PbS quantum dot solids. *Materials* **2015**, *8*, 1858–1870.

(25) Kramer, I. J.; Sargent, E. H. The architecture of colloidal quantum dot solar cells: materials to devices. *Chem. Rev.* **2014**, *114*, 863–882.

(26) Tavakoli, M. M.; Simchi, A.; Fan, Z.; Aashuri, H. Chemical processing of three-dimensional graphene networks on transparent conducting electrodes for depleted-heterojunction quantum dot solar cells. *Chem. Commun.* **2016**, *52*, 323–326.

(27) Ning, Z.; Voznyy, O.; Pan, J.; Hoogland, S.; Adinolfi, V.; Xu, J.; Li, M.; Kirmani, A. R.; Sun, J. P.; Minor, J.; et al. Air-stable n-type colloidal quantum dot solids. *Nat. Mater.* **2014**, *13*, 822–828.

(28) Tang, J.; Kemp, K. W.; Hoogland, S.; Jeong, K. S.; Liu, H.; Levina, L.; Furukawa, M.; Wang, X.; Debnath, R.; Cha, D.; et al. Colloidal-quantum-dot photovoltaics using atomic-ligand passivation. *Nat. Mater.* **2011**, *10*, 765–771.

(29) Pattantyus-Abraham, A. G.; Kramer, I. J.; Barkhouse, A. R.; Wang, X.; Konstantatos, G.; Debnath, R.; Levina, L.; Raabe, I.; Nazeeruddin, M. K.; Grätzel, M.; et al. Depleted-heterojunction colloidal quantum dot solar cells. *ACS Nano* **2010**, *4*, 3374–3380.

(30) Brown, P. R.; Kim, D.; Lunt, R. R.; Zhao, N.; Bawendi, M. G.; Grossman, J. C.; Bulović, V. Energy level modification in lead sulfide quantum dot thin films through ligand exchange. *ACS Nano* **2014**, *8*, 5863–5872.

(31) Vo, N. T.; Ngo, H. D.; Vu, D. L.; Duong, A. P.; Lam, Q. V. Conjugation of E. coli O157: H7 antibody to CdSe/ZnS quantum dots. *J. Nanomater.* **2015**, *2015*, 1–7.

(32) Liu, M.; Voznyy, O.; Sabatini, R.; García de Arquer, F. P. G.; Munir, R.; Balawi, A. H.; Lan, X.; Fan, F.; Walters, G.; Kirmani, A. R.; et al. Hybrid organic-inorganic inks flatten the energy landscape in colloidal quantum dot solids. *Nat. Mater.* **2016**, *16*, 258–263.

(33) Semonin, O. E.; Luther, J. M.; Choi, S.; Chen, H. Y.; Gao, J.; Nozik, A. J.; Beard, M. C. Peak external photocurrent quantum efficiency exceeding 100% via MEG in a quantum dot solar cell. *Science* **2011**, *334*, 1530–1533.

(34) Kiani, A.; Sutherland, B. R.; Kim, Y.; Ouellette, O.; Levina, L.; Walters, G.; Dinh, C. T.; Liu, M.; Voznyy, O.; Lan, X.; et al. Single-step colloidal quantum dot films for infrared solar harvesting. *Appl. Phys. Lett.* **2016**, *109*, 183105.

(35) Tavakoli, M. M.; Tavakoli, R.; Hasanzadeh, S.; Mirfasih, M. H. Interface engineering of perovskite solar cell using a reduced-graphene scaffold. *J. Phys. Chem. C* **2016**, *120*, 19531–19536.

(36) Tavakoli, M. M.; Tsui, K. H.; Zhang, Q.; He, J.; Yao, Y.; Li, D.; Fan, Z. Highly efficient flexible perovskite solar cells with antireflection and self-cleaning nanostructures. *ACS Nano* **2015**, *9*, 10287–10295.

(37) Moreels, I.; Justo, Y.; De Geyter, B.; Haustraete, K.; Martins, J. C.; Hens, Z. Size-tunable, bright, and stable PbS quantum dots: a surface chemistry study. *ACS Nano* **2011**, *5*, 2004–2012.

(38) Tavakoli, M. M.; Simchi, A.; Aashuri, H. Supercritical synthesis and in situ deposition of PbS nanocrystals with oleic acid passivation for quantum dot solar cells. *Mater. Chem. Phys.* **2015**, *156*, 163–169.

(39) Tavakoli, M. M.; Mirfasih, M. H.; Hasanzadeh, S.; Aashuri, H.; Simchi, A. Surface passivation of lead sulfide nanocrystals with low electron affinity metals: photoluminescence and photovoltaic performance. *Phys. Chem. Chem. Phys.* **2016**, *18*, 12086–12092.

(40) Tavakoli, M. M.; Tavakoli, R.; Davami, P.; Aashuri, H. A quantitative approach to study solid state phase coarsening in solder alloys using combined phase-field modeling and experimental observation. *J. Comput. Electron.* **2014**, *13*, 425–431.

(41) Leung, S. F.; Zhang, Q.; Tavakoli, M. M.; He, J.; Mo, X.; Fan, Z. Progress and design concerns of nanostructured solar energy harvesting devices. *Small* **2016**, *12*, 2530–2530.

(42) Tavakoli, M. M.; Lin, Q.; Leung, S. F.; Lui, G. C.; Lu, H.; Li, L.; Xiang, B.; Fan, Z. Efficient, flexible and mechanically robust perovskite solar cells on inverted nanocone plastic substrates. *Nanoscale* **2016**, *8*, 4276–4283.

(43) Lin, Q.; Lu, L.; Tavakoli, M. M.; Zhang, C.; Lui, G. C.; Chen, Z.; Chen, X.; Tang, L.; Zhang, D.; Lin, Y.; et al. High performance thin

film solar cells on plastic substrates with nanostructure-enhanced flexibility. *Nano Energy* **2016**, *22*, 539−547.

(44) Yu, R.; Ching, K. L.; Lin, Q.; Leung, S. F.; Arcrossito, D.; Fan, Z. Strong light absorption of self-organized 3-D nanospike arrays for photovoltaic applications. *ACS Nano* **2011**, *5*, 9291−9298.

(45) Kapadia, R.; Fan, Z.; Javey, A. Design constraints and guidelines for CdS/CdTe nanopillar based photovoltaics. *Appl. Phys. Lett.* **2010**, *96*, 103116.